1   **Can Whole Building Energy Models Outperform Numerical Models, When**

2   **Forecasting Performance of Indirect Evaporative Cooling Systems?**

3   A. Badiei[1,*], Y. G. Akhlaghi[1], X. Zhao[1], J. Li[1], F. Yi[1], Z. Wang[1,2]

4   [1]Research Centre for Sustainable Energy Technologies, Energy and Environment Institute,
5   University of Hull, Hull, HU6 7RX, UK

6   [2]School of Civil and Transportation Engineering, Guangdong University of Technology,
7   Guangzhou, P.R. China, 510006

8   *Corresponding author: A.Badiei@Hull.ac.uk; Tel.: +44 (0) 1482 86 3611

9   **Abstract**

10   This paper presents a whole building energy modelling work incorporating a state-of-the-art
11   indirect evaporative cooling system. The model is calibrated and validated with real-life
12   empirical data, and is capable of representing actual performance of the system with high
13   reliability. The investigated system is a novel super-performance Dew Point Cooler (DPC)
14   with a guideless and corrugated Heat and Mass Exchanger (HMX). The DPC is modelled as
15   part of the whole building energy model through detailed description of system and building
16   characteristics at source code level. The developed model has been simulated in all different
17   climates that an Indirect Evaporative Cooling (IEC) system can be operated, namely:
18   subtropical hot desert, humid continental, Mediterranean, and hot desert climates. The
19   performance predictions has been tested against experiments and numerical model of the
20   same system, and a detailed investigation of modelling approaches to efficiently and
21   effectively model aforementioned systems has been provided.

22   The calibrated and empirically validated whole building energy model predicted the key
23   performance parameters of the dew point evaporative cooling system with mean error values
24   limited to 4.1%. The highest COP values recorded by experiments and whole building
25   energy simulations were 51.1 and 49, respectively. The whole building energy model proved
26   to better predict the performance of dew point evaporative cooler, when compared to
27   numerical models, by incorporating the building-side parameters into the model. This
28   modelling work paves the way toward detailed investigation of the advanced cooling systems
29   within building context to achieve optimised performance of the system in wide range of
30   buildings and operating conditions.

31   ***Keywords:*** *Dew Point Cooler; Building energy; Model; Performance; Experiment*

1. Introduction

1.1. Background

The rapid growth in global energy consumption, especially in past decades, has raised the world-wide concern over security of supply as the existing energy resources are exhausting [1]. One of the main contributors to the rising global energy consumption is the service sector which covers all the commercial and public buildings with a wide range of HVAC system [2]. The global energy consumption of service sector has increased by 295 Mtoe in 2018 compared to 2000 levels and with this trend the sector would consume a further 323 Mtoe by 2040. The sector has also showed the least reduction potential in energy consumption under the Sustainable Development Scenario, compared to Industry, Residential and Transport sectors [1]. To deal with the high energy consumption levels associated with the service sector and to improve its poor performance under future scenarios, the focus has been shifted toward development of advanced, efficient and low-energy HVAC solutions in recent years.

The growing energy use by HVAC systems are particularly significant in developed countries. In the USA, HVAC energy use accounts for up to 50% of building energy consumption [3] while in china the HVAC energy use is between 50-70% of the total energy consumed in buildings [4]. Issac and Vuuren [5] estimated that energy demand associated with air-conditioning will rise rapidly in 21st century reaching a peak of 4000 TWh in 2050 and more than 10,000 TWh by 2100. There are other studies which have predicted a similar rise in energy demand of air-conditioning [6] under future weather conditions of USA [7], Switzerland [8], and Australia [9].

1.2. Air-conditioning: past, present and future

Traditionally, the most dominant air-conditioning systems were Mechanical Vapour Compression (MVC) ones which due to their inefficient compressors consumed a considerable amount of electricity [10]. In past decades absorption and adsorption cooling systems have gained more interest over mechanical vapour compression systems due to their lower energy consumption. The absorption and adsorption cooling systems greatly owe their lower energy consumption to replacing energy-intensive compressor with a cycle of high temperature water or vapour which reduces the applicability of these systems in sites with no access to heat source. Complexity of the pressurised and de-pressurised units used in the absorption and adsorption cooling systems and high maintenance costs associated

64 with them are other shortcomings of these systems which have raised the need for practical
65 solutions [11].

66 The most recent approach to provide conditioned air is based on the fundamentals of
67 evaporative cooling which relies on latent heat of water (both recyclable and renewable) to
68 remove dissipated heat from conditioned spaces. The Dew Point Evaporative Cooling
69 approach was first investigated by Dr Valeriy Maisotsenko [12] and the resultant technology
70 is adeptly known as M-cycle cooling [3]. Evaporative cooling systems generally fall under
71 two categories: Direct Evaporative Cooling (DEC) and Indirect Evaporative Cooling (IEC)
72 based on whether the primary air is in direct contact with cooling water or not. In DECs, the
73 direct contact between primary air and cooling water results in production of cooled but more
74 humid air which provides reduced occupant comfort and is not suitable for high-tech facilities
75 like data centres. IECs, on the other hand, separate the primary air and the cooling water by
76 introducing dry and wet channels which cools the product air through the heat transfer
77 between the two channels [13]–[15]. While IECs provide better indoor air quality compared
78 to DECs, they have a lower heat removal capacity due to the constraints introduced by air's
79 wet-bulb temperature.

80 To overcome the shortcomings of IECs, Dew Point Coolers (DPC) as the most advanced
81 indirect evaporative cooling systems available in the market, offer a modified heat and mass
82 exchanger (HMX) configuration to provide pre-cooling for the air in wet channels, eliminate
83 the wet-bulb limits, and lower the product air temperature down to its dew point, thus
84 improving the cooling efficiency by up to 30% compared to conventional IECs [3], [16]–[19].

85 *1.3. Dew Point Coolers*

86 The research on Dew Point Coolers (DPCs) has gained more interest in past decade with
87 first published work dating back to 2006 by Coolerado® project in USA [16] where a cross-
88 flow HMX DPC with perforated holes on the flow path was tested. Results indicated that by
89 employing this type of HMX, for the first time, wet-bulb and dew-point effectiveness of up to
90 80% and 50%, respectively could be achieved under specific operational conditions [16].
91 Since the first successful investigation and implementation of DPCs, more research has
92 considered the potentials of these advanced cooling systems and recorded wet-bulb and
93 dew-point effectiveness has reached values as high as 114% and 84%, respectively by
94 Riangvilaikul et al. [20]. In their study a novel, vertically positioned DPC with counter-flow
95 configuration between the intake and working air, and between the working air and water
96 was tested experimentally.

97 Other example of experimental works on DPCs is a flat-plate cross-flow HMX DPC by Bruno
98 [21] that used a special sheet with high water retention and wicking capability as the wet
99 material layer, and a water-proof membrane as a dry material layer. The authors reported
100 they were able to achieve an average dew-point effectiveness of 75%, which was relatively
101 higher than that of the existing types for the same operational conditions. Xu et al. [4]
102 performed an experimental analysis of a DPC prototype employing a super performance wet
103 material, intermittent water supply configuration and a corrugated HMX to find wet-bulb and
104 dew-point effectiveness of up to 114% and 75%, respectively, and a record-high COP of
105 52.5. The performance of same prototype DPC was then examined by Akhlaghi et al. [22]
106 under four different climatic conditions, namely humid continental, Mediterranean, sub-
107 tropical hot desert, and hot desert climates. Annual energy savings of up to 90% was
108 achieved compared to the conventional MVCs.

109 With increasing demand for even more efficient and low-energy DPCs various modelling
110 techniques and simulation tools have been employed by researchers across the world to
111 investigate complex HMX configurations, water supply patterns, dry and wet channel
112 materials, varying operating conditions and space requirements [20]–[36]. The modelling
113 research on DPCs is investigated critically in the next section with particular attention to
114 experimental validation of model outputs and observed uncertainties, advantages and
115 limitation various modelling approaches introduce, and how this study fills the existing
116 research gap on DPC research topic.

117 *1.4. Modelling DPCs: advantages, limits and the gap*

118 The vast majority of research on DPCs has employed numerical modelling techniques.
119 Hasan [30] employed an analytical model of a regenerative indirect evaporative cooling
120 trying to achieve sub-wet bulb temperature without the need for a vapour compressor. The
121 results of analytical model was compared with a previously developed numerical model and
122 some tests, and the recorded agreement of results ensured validity of system performance
123 modelling [30]. Cui et al. also developed a numerical model of a evaporative dew point
124 cooler [32] and investigated the performance of system under three improved scenarios
125 namely, varying channel dimensions; employing room return air as the working fluid; and
126 installation of physical ribs along the channel length [37]. Their model was validated through
127 comparison of temperature distribution and outlet air conditions with experimental results,
128 and the largest discrepancy was recorded as ±7.5%.

129 Lin et al. [33] employed a transient and dynamic numerical model to take into account the
130 dynamic transitions between various components of a DPC and validated the model through

131   inter-model comparison with a steady-state model of the same DPC and experimental
132   comparison which yielded 4.3% discrepancy. Pandelidis et al. performed two numerical
133   studies, one to investigate heat and mass transfer processes in an M-cycle HMX of a DPC
134   [34] and the other to optimize the performance of the same evaporative air cooler [35]. In
135   both studies experimental data was used to ensure the validity of model results and the
136   optimal range of operational and geometrical conditions were identified. Akhlaghi et al. [38]
137   developed a statistical model of a novel DPC employing Multiple Polynomial Regression
138   (MPR) technique to predict the performance of the system. Several operating parameters
139   including intake air temperature, relative humidity and flow rate as well as overall cooling
140   capacity, Coefficient of Performance (COP), and wet bulb efficiency were investigated before
141   applying the model to a number of scenarios in dry climates.

142   Sohani et al. [36] used a Neural Network (NN) based numerical model to study and optimise
143   the performance of a DPC with M-cycle under 12 diverse climatic weather conditions. While
144   the multi-objective optimisation technique used by authors was able to improve mean values
145   of the COP and cooling capacity by 8.1% and 6.9%, adequate evidence on empirical
146   validation of the model was not provided. Chen et al. [24] employed a experimentally
147   validated numerical model of an IEC to perform a detailed sensitivity analysis and
148   optimisation based on the most influential and practically controllable parameters. Xu et al.
149   [28] also did a numerical modelling work on guideless irregular HMX with corrugated heat
150   transfer surface as used in a novel DPC. The experimentally validated work proved that the
151   novel DPC system was capable of achieving up to 37% more cooling capacity, 55.8% higher
152   wet bulb efficiency, and 33.3% higher COP.

153   Other studies by Moshari and Heidarnejad [23], Akhlaghi et al. [39], [22], Riangvilaikul [20],
154   [26], and Jradi et al. [27] all performed some sort of numerical modelling exercise in IECs
155   and validated their findings through comparison with experimental data and other models.
156   While all these studies were successful in recording some or extraordinary improvements in
157   performance of the investigated systems, the vast majority of improvements were recorded
158   under controlled test conditions in laboratory environment, neglecting the extensive building
159   and occupants' interactions which happen in real world.

160   This study, therefore, fills the existing gap in DPC research by investigating the performance
161   of a novel dew point evaporative cooling system through whole building energy modelling
162   where the restraining system interactions with hosting building and its occupants are
163   captured. In this way the transient behaviours of the system within the building envelope are
164   quantified and the resultant impact on performance parameters of the system is investigated.
165   A comparison of the predicted performance parameters from whole building energy

166   simulation to those from numerical models of the same system enabled the critical

167   assessment of each modelling approach in dealing with advanced Indirect Evaporative

168   Cooling (IEC) systems.

169   ## 2. System Description

170   This study investigates a state-of-the-art, high-performance counter flow DPC employing a

171   complex, 4 kW rated Heat and Mass Exchanger (HMX). The new HMX configuration

172   replaces the channel support guides with a corrugated heat transfer surface separating dry

173   and wet channels (as depicted in **Figure 1**) which decreases air flow resistance by up to

174   56% and increases heat transfer area by up to 40% leading to an improved heat transfer

175   rate [28]. As seen in Figure 1 (a), a number of perforated holes are designed on top of each

176   corrugated sheet to allow partial flow of air from dry channels to wet ones in order to

177   complete heat transfer cycle and cool down the air in dry channels. The dry channels are

178   made of a specific aluminium with high malleability while the wet channels' material is a

179   flexible *Coolmax®* fibre with high water absorption, diffusion and evaporation capacities

180   which allows the sheet to have corrugated shape. The geometric dimensions of the HMX is

181   summarised in **Table 1**.

182   When system operates, the air with relatively high temperature and moisture level enters the

183   DPC and passes through the dry channel losing its heat to the adjacent wet channel

184   reducing its temperature to the desired level. Upon reaching the end of dry channel a part of

185   cooled air leaves the channel as product air (to the conditioned space) and the remaining air

186   is transferred to the wet channels through perforated holes as working air. This working air

187   then gains heat from adjacent dry channel and moisture from *Coolmax®* material while

188   passing through the wet channel and is discharged as exhaust air and water drops. In

189   comparison to conventional flat plate HMXs, the introduced HMX configuration reduces the

190   airflow resistance, increases heat transfer area, has higher diffusion area and better

191   evaporation owing to use of *Coolmax®* wet channel material.
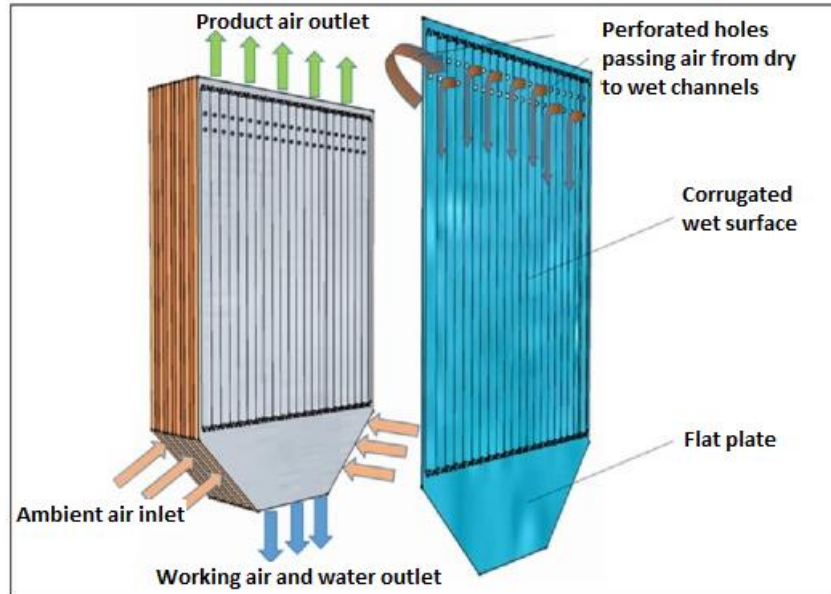
192 **Figure 1** Heat and Mass Exchanger (HMX). Upper: configuration and structure, Lower:
193 corrugated heat transfer surfaces separating dry and wet channels [38]

194 Owing to the high absorption capacity of fibrous material in the wet channels, the intermittent
195 water supply scheme was used by a dedicated water distributer system, which reduces the
196 amount of water used as well as water pump power consumption. The water distributer is
197 composed of a water pump, a water header, a water sink, and a water distributer tubes
198 which enable the even distribution of water over the surface of wet channels. When the
199 water sink underneath the HMX is empty, the water is supplied with flow rate of 6.85 L/min
200 for 15 seconds with 10 minutes intervals, and when the tank is full, the water is supplied with
201 flow rate of 2.45 L/min for 60 seconds with 10 minutes intervals.

202 In addition to the complex HMX introduced above, the DPC also employs two supply and
203 two exhaust air fans each with 160 W power, 458 Pa pressure, and 705 m^3/h volumetric flow
204 rate, one circulating water pump with 24V DC power and 450 L/h flow rate, and two

205 controllers for the fans and the water pump. **Table 2** summarises the key elements of the
206 DPC system and associated technical specifications.

207 <center>**Table 1** Geometric dimensions of the Heat and Mass Exchanger</center>

Inlet flat plate height	120	mm
Outlet flat plate height	10	mm
Corrugated plate height	860	mm
Transition length between flat and corrugated plates height	5*	mm
Number of corrugated plates	160	-
Total height of the HMX	1000	mm
Width	800	mm
Length	358	mm
Total heat transfer area	49.3	m^2
Height of corrugated wave	2.8	mm
Width of corrugated wave	11.6	mm

*on each of the inlet and outlet sides

208 **Table 2** Technical manufacturer specifications of the DPC components

Component	Specifications
Supply air fan	R3G225-RE07-03, ebm-papst Ltd, fan speed 2865 rpm, 705 m3 .h^{-1}, 458 Pa, 160 W
Exhaust air fan	R3G225-RE07-03, ebm-papst Ltd, fan speed 2865 rpm, 705 m3 .h^{-1}, 458 Pa, 160 W
Water pump	DH40H-24110, Shenzhen Zhongke Century Technology, 24 V/1.2 A DC, 11mH$_2$O, 450 L/hr
Fan controller	980-CAS11007 – TMS Controller, ebm-papst Ltd
Pump controller	DH48S-S, Xinling Electrical Co. Ltd

209 **Figure 2** represents the whole system design, the computer model, and the actual system in
210 the laboratory environment.
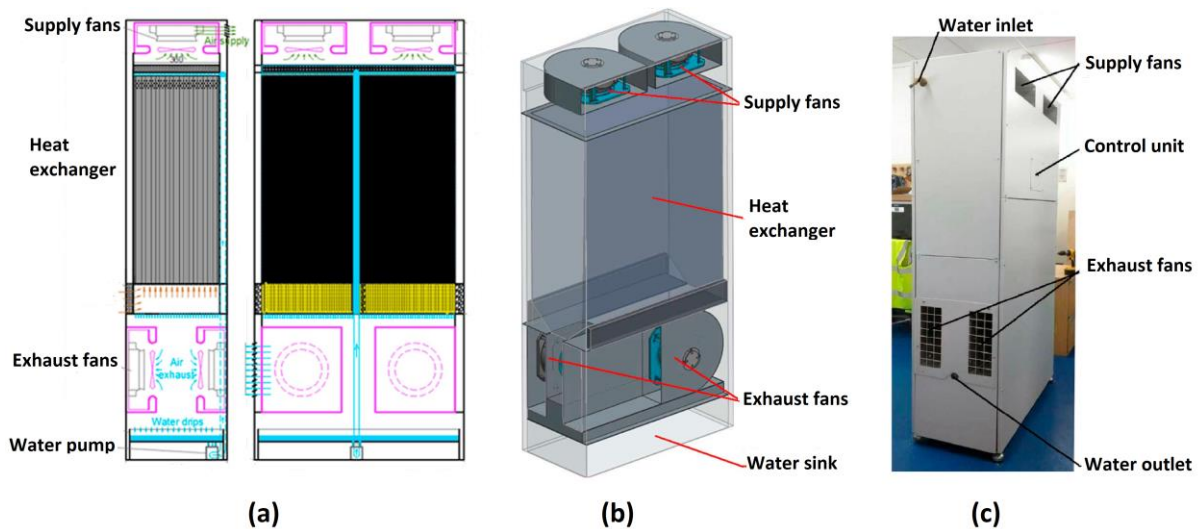
Figure 2 Dew Point Cooler (DPC) and its components. (a): 2D cross-section view, (b) 3D computer model, (c): actual system in the lab environment [4]

Finally, for optimum operation of the DPC, temperature of the running water is kept at the range of 16-20˚C to ensure efficient cooling [4]. A water filter with cartridge to purify the water and an anti-scale agent was used to minimise the risk of blockage at the perforated holes. Also an optimised water distribution scheme was introduced to maximise the use of circulating water within the cooler and reduce the amount of intake water [4].

3. Experimental Set-up and Analysis Method

To examine performance of the novel 4 kW Dew Point Cooler (DPC) with introduced complex Heat and Mass Exchanger (HMX), the test set-up presented in **Figure 3** was constructed in the lab environment. The test set-up comprises a heater, a humidifier/dehumidifier, and four balancing dampers to enable conditioning of the inlet air and simulate various weather conditions.

The water pump, supply and exhaust fans, and supply-discharge ducting system is also presented in **Figure 3.** After conditioning the inlet air temperature and humidity to match those of the climates under study, the supply fans and the necessary ducting is used to create a zero static pressure at the inlet of DPC. A specific multi-function measurement device capable of measuring the ventilation and air conditioning parameters as well as indoor air quality parameters (i.e. temperature, humidity, flow rate and speed) was used to identify the characteristics of the air flow at the inlet and outlet of the system. The measurement points were placed at a distance 10 times the diameter of the ducts (⌀160 mm) from inlet and outlet of the system to allow development of fully steady air flow for the sake of accuracy of measurements. Two water flow meters were also installed at the inlet

235 and outlet of wet channels to measure the amount of water used and consequent pressure
236 drop. A water pressure of 1.8 mH$_2$O was preserved throughout the system to ensure even
237 distribution of the water across the wet surfaces (as suggested by *Coolmax®* wet channel
238 material manufacturer). Finally, a simple fan controller was employed to achieve the
239 optimum working air to intake air ratio of 0.37, and product air and waste air flow rates of 602
240 m^3.h^{-1} and 364 m^3.h^{-1}, respectively, throughout the experiments as identified by [20].
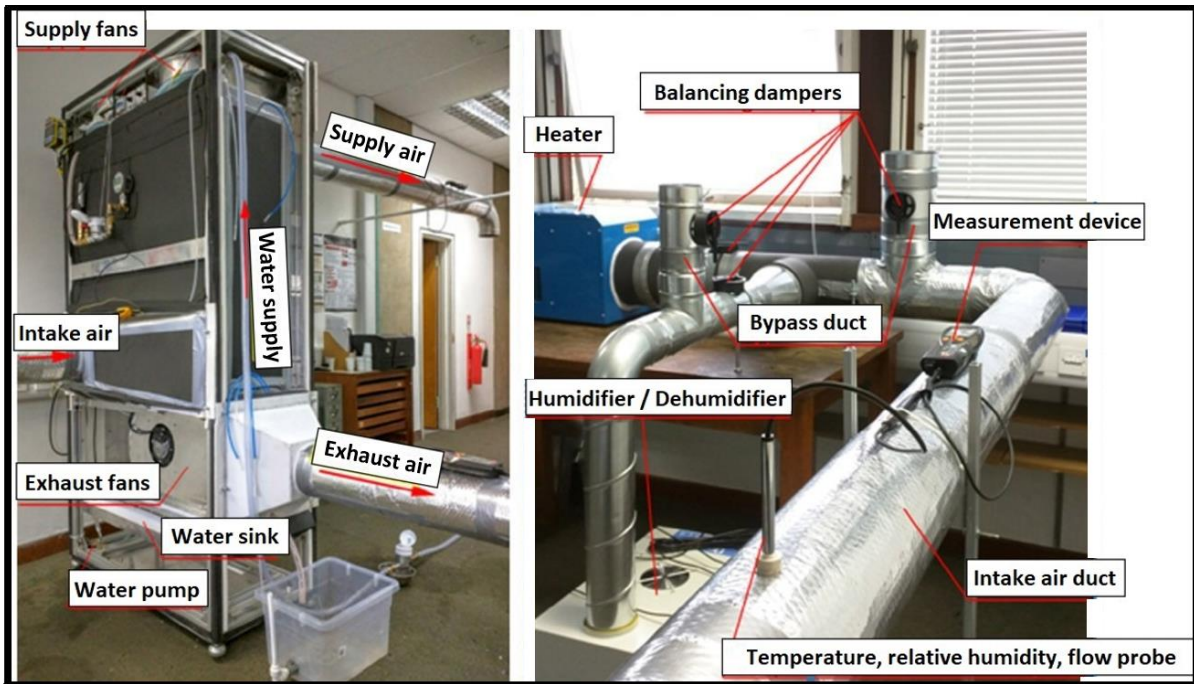
241

242 **Figure 3** Experimental test set-up with individual components as constructed in the
243 laboratory environment

244 The measure parameters from the system are recorded in real time and analysed to quantify
245 the overall cooling capacity, Coefficient of Performance (COP), wet bulb and dew point
246 efficiencies. The overall cooling capacity of the system can be calculated from **Equation 1**,
247 as suggested by ASHRAE [40] for all Indirect Evaporative Cooling (IEC) systems:

$$Q_{Cooling} = C_p(T_{dry,in} - T_{dry,out})(1 - \varphi)Q_{m,dry,in}$$ **Equation 1**

248 Where $Q_{Cooling}$ is the cooling capacity of DPC, C_p is the specific heat capacity of the inlet
249 air, $T_{dry,in}$ and $T_{dry,out}$ are the inlet and outlet temperatures of the air in dry channel, φ is
250 the working air to intake air ratio, and $Q_{m,dry,in}$ is the mass flowrate of the intake air in the
251 dry channel.

252 Then the Coefficient of Performance (COP) can be calculated as the ratio of cooling capacity
253 to the total of electrical power consumed by fans (W_{Fans}) and pumps (W_{Pumps}):

$$COP = \frac{Q_{Cooling}}{W_{Fans} + W_{Pumps}}$$ **Equation 2**

254 Finally, the wet bulb and dew point efficiencies (ε_{wb} and ε_{dp}) are calculated from **Equation 3**
255 and **Equation 4**, respectively:

$$\varepsilon_{wb} = \frac{T_{dry,in} - T_{dry,out}}{T_{dry,in} - T_{dry,in,wb}}$$ **Equation 3**

$$\varepsilon_{dp} = \frac{T_{dry,in} - T_{dry,out}}{T_{dry,in} - T_{dry,in,dp}}$$ **Equation 4**

256 Where $T_{dry,in,wb}$ and $T_{dry,in,dp}$ are the wet-bulb temperature of the intake air in dry channel
257 and the dew point temperature of the intake air in dry channel, respectively.

258 Having identified the performance parameters needed to investigate the DPC, four
259 representative cities with totally different weather conditions were identified to test the
260 performance of system. These cities are: Las Vegas (USA) with subtropical hot desert
261 climate, Beijing (China) with humid continental climate, Rome (Italy) with Mediterranean
262 climate, and Riyadh (KSA) with hot desert climate. The weather conditions from these cities
263 were simulated and corresponding intake air with representative temperature and humidity
264 levels were produced in the laboratory environment to test the performance of DPC under
265 each climate. Due to very high relative humidity of the air in Beijing and Rome, a pre-
266 treatment had to been applied to the intake air in order to bring the humidity level to the
267 operational range (<40%) of the DPCs in common high-tech facilities like data centres [39].
268 Hence, this research could focus solely on the cooling performance of the system without
269 having to take into account the dehumidification. The dehumidification process was carried
270 out using a solar/waste energy driven dehumidification cycle employing a desiccant bed
271 located inside a channel that is constructed by a porous and visible-light LiCl-Sillicon-Gels
272 material. As a result of the dehumidification process, the moisture content of outside air in
273 Beijing and Rome are brought down required range resulting in a parallel sensible cooling
274 process. The monthly average temperature and relative humidity of the four representative
275 cities and corresponding pre-treated values for Beijing and Rome are all summarised in
276 **Table 3**.

As seen in **Table 3** the temperature and humidity values are given only for the months where free cooling is not available in each particular climate and there is need for operation of DPC. The average outdoor temperature required for free cooling is identified as 22°C based on ASHRAE guidelines for power requirements in data centre design [41]. For Beijing and Rome weather conditions where pre-treatment was necessary, the pre-treated monthly temperatures are taken as the selection criteria. Hence, the DPC operation is required from March to October in Riyadh, from April to October in Beijing and Las Vegas, and from May to October in Rome as seen in **Table 3**.

Table 3 Monthly average temperature and humidity values for the four representative cities with pre-treatment data where required

Month	Beijing				Rome				Las Vegas		Riyadh	
	Before pre-treatment		After pre-treatment		Before pre-treatment		After pre-treatment		No pre-treatment needed			
	T(°C)	RH	T(°C)	RH	T(°C)	RH	T(°C)	RH	T(°C)	RH	T(°C)	RH
March	-	-	-	-	-	-	-	-	-	-	27	37%
April	20	45%	23.7	16%	-	-	-	-	25	25%	31	35%
May	26	53%	30.8	23%	23	75%	27.3	39%	30	21%	38	21%
June	30	60%	35.6	24%	26	74%	30.8	35%	37	18%	42	16%
July	31	75%	36.8	24%	28	73%	33.2	38%	40	20%	44	17%
August	30	78%	35.6	40%	28	75%	33.2	39%	39	27%	42	19%
September	27	69%	32	35%	27	75%	32	39%	33	26%	42	19%
October	20	60%	23.7	28%	23	76%	27.3	40%	27	30%	35	23%

Having identified the intake air properties, the heater and humidifier/dehumidifier shown in **Figure 3** were used to produce the intended intake air for the DPC and then the DPC was operated under each weather conditions. The system performance parameters as well as the achieved indoor air properties were recorded and are presented in **Section 6**.

4. Numerical Model of the System

A numerical model of the advanced Dew Point Cooler (DPC) with corrugated HMX design was developed using Multiple Polynomial Regression (MPR) technique [38]. Regression analysis is a very popular and well know method as it provides robust grounds for developing predictive tools to investigate complex relations between dependant and

296 independent parameters in a wide range of areas i.e. engineering, physics and chemical
297 sciences [42], [43]. The developed model takes a set of operational and geometric
298 parameters as input to predict the performance parameters of the DPC under investigation.
299 These parameters and their corresponding ranges as used in the MPR model are
300 summarised in **Table 4**.

301 **Table 4** Operational and geometrical parameters used in the MPR model to predict
302 performance parameters of the DPC and the corresponding ranges

Operational Parameters	Range	Geometrical Parameters	Range	Performance Parameters
Intake air temperature, T(°C)	25-45	Channel height, H (m)	1-3	Cooling capacity
Intake air relative humidity, RH	0.125-0.5	Channel interval, Int (m)	0.004-0.008	Coefficient of Performance
Intake air flow rate, U (m/s)	0.3-3.3	Number of layers, L	100-200	Dew point effectiveness
Working air to intake air ratio (φ)	0.1-0.9	-	-	Wet-bulb effectiveness

303 The operating and geometrical parameters were used as independent parameters in the
304 MPR model mainly due to the flexibility of these parameters which allows them to be
305 changed continuously in real-life operation of the DPC. Hence, other parameters which didn't
306 offer such flexibility were excluded from input parameters of the model.

307 **Table 5** Discrete values selected for operating parameters to construct training and
308 validation sets of the MPR model [38]

No	Training set				Validation set			
	T (°C)	RH	U (m/s)	φ	T (°C)	RH	U (m/s)	φ
1	25	0.125	0.3	0.1	26.25	0.14	0.5	0.15
2	27.5	0.17	0.7	0.2	28.75	0.19	0.9	0.25
3	30	0.22	1.1	0.3	31.25	0.24	1.3	0.35
4	32.5	0.26	1.5	0.4	33.75	0.28	1.7	0.45
5	35	0.3	1.9	0.5	36.25	0.32	2.1	0.55
6	37.5	0.34	2.3	0.6	38.75	0.36	2.5	0.65
7	40	0.38	2.7	0.7	-	-	-	-
8	42.5	0.42	3	0.8	-	-	-	-
9	45	0.5	3.3	0.9	-	-	-	-

309   Having identified the input (operational and geometrical) parameters and their ranges,

310   discrete values for each parameter were required to construct a training set to develop the

311   model and a validation set to verify the developed model. Hence, 9 discrete values for the

312   training set and 6 discrete values for the validation set were selected to develop the MPR

313   model (**Table 5**).

314   As seen in **Table 5** the discrete values for the two sets were chosen such that the validation

315   set values won't overlap with training set values, hence offering robust model validation

316   grounds. As for geometrical parameters, discrete values of 1m, 2m, and 3m for height,

317   0.0004m and 0.008 for interval, 100 and 200 for number of layers were used in the model

318   (see **Figure 1** for geometrical parameters). Water temperature was modelled as 16˚C and

319   water flow rate as 411 L/h to match the experimental values [4]. All the possible

320   combinations with these discrete values were considered in the model to account for all the

321   random operating conditions. Hence, the total number of operating conditions becomes 7857

322   in which 80% of them, 6561 (9^4), are for training set and 20%, 1296 (6^4), are for the

323   validation set. Once the model is developed and validated, it can be used beyond the scope

324   of the discrete values and ranges presented in **Table 4** and **Table 5**.

325   The regression model was developed from the described data sets in R software package

326   can be represented in the following equation:

$$
\begin{aligned}
Y = \ & \beta_0 + \beta_1 \times (T^{n_{1,1}} \times RH^{n_{2,1}} \times U^{n_{3,1}} \times \varphi^{n_{4,1}}) \\
& + \beta_2 \times (T^{n_{1,2}} \times RH^{n_{2,2}} \times U^{n_{3,2}} \times \varphi^{n_{4,2}}) + \cdots \\
& + \beta_m \times (T^{n_{1,m}} \times RH^{n_{2,m}} \times U^{n_{3,m}} \times \varphi^{n_{4,m}})
\end{aligned}
$$
Equation 5

327   Where Y represents all the performance parameters to be predicted by model, T is

328   temperature, RH is the relative humidity, U is air flow velocity of intake air, and φ is the

329   working air to intake air ratio. β_0, β_1, β_2, …, β_m are regression coefficients to represent

330   geometric characteristics; $n_{1,m}$ represents the intake air temperature of the mth coefficient,

331    $n_{2,m}$ represents intake air humidity of the mth coefficient, $n_{3,m}$ represents intake air flow

332   velocity of the mth coefficient, and $n_{4,m}$ represents the working air to intake air ratio of the mth

333   coefficient.

334   The model was developed based on the introduced training sets and the validation set was

335   used to verify the predicted performance parameters (Y). For validation purpose, least

336   squares method was used where the sum of squared residuals are minimised. The residual

337   or Sum Square of Errors (SSE) is the difference between the actual values and the

338   estimated regression values by MPR model (also denoted as r_i):

$$SSE = \sum_{i=0}^{N}(\hat{Y}_i - Y_i)^2 = \sum_{i=0}^{N} r_i{}^2$$

Equation 6

339 Where $\hat{Y}$ represents the predicted value of individual performance parameters, Y is the
340 actual value of the same parameter, and N is the number of predicted value. Having
341 identified the SSE value, three of the main metrics to evaluate the performance of the model
342 i.e. Mean Square Error (MSE), Maximum Relative Error (MRE), and coefficient of
343 determination (R^2) can be calculated:

$$MSE = \frac{SSE}{N} = \frac{\sum_{i=0}^{N}(\hat{Y}_i - Y_i)^2}{N} = \frac{\sum_{i=0}^{N} r_i{}^2}{N}$$

Equation 7

$$R^2 = 1 - \frac{SSE}{SST} = 1 - \frac{\sum_{i=0}^{N}(\hat{Y}_i - Y_i)^2}{\sum_{i=0}^{N}(\overline{Y}_i - Y_i)^2}$$

Equation 8

344 Where SST is sum square of total, and $\overline{Y}$ is the mean of predicted values.

5. Whole Building Energy Model

346 The whole building dynamic energy model of the system and the hosting building was
347 developed using EnergyPlus (e^+) software package (version 8.9.0.1) [44], which is open
348 source, widely used and verified. In order to enable empirical validation and comparison with
349 numerical model, the same system parameters and numerical model inputs as described in
350 **Sections 2**, **3** and **4** were used in developing the whole building energy model. Where there
351 was lacking data, further data collection was conducted to create a detailed energy model
352 which is capable of representing reality with high reliability.

353 To facilitate the data input process, DesignBuilder [45] software version 6.1.2.009 was
354 employed to create laboratory building's geometry (where DPC was operated and tested),
355 construction materials, internal boundary conditions and a template of an Indirect
356 Evaporative Cooler (IEC). DesignBuilder was used initially because it is a commercially
357 available software package that offers detailed dynamic thermal simulations, employing the
358 EnergyPlus simulation engine and provides a user friendly graphical user interface [45].

359 Having formed the basis for energy model of the DPC in Laboratory environment, the
360 corresponding EnergyPlus Input Data File (IDF) was exported with *.idf* extension. The IDF
361 was then modified using a text editor and the EnergyPlus IDF editor [46] to add exact DPC
362 characteristics as described in **Sections 2** and **3** (**Figure 4**). The completed IDF with custom
363 weather files created for the four cities investigated in the experiments (see **Table 3** for

364 details) were fed to the EnergyPlus and simulations were run. As seen in **Figure 4** the

365 simulation results were then checked against experimental results and necessary

366 modification were added to the EnergyPlus IDFs in order to produce the validated and

367 calibrated model of the DPC under investigation.
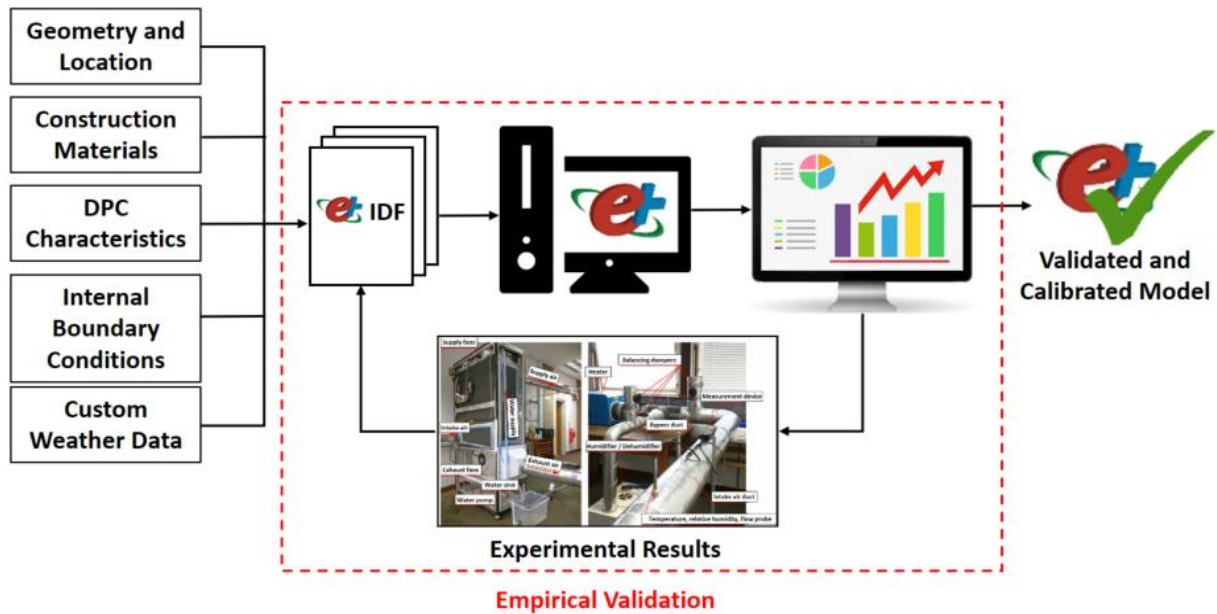
368

369 **Figure 4** Schematic of the whole building energy modelling process: from raw data to the

370 validated model

371 Upon completion of the modelling process as depicted in **Figure 4**, the validated whole

372 building energy model and the performance parameters predictions are compared to the

373 numerical model estimates (**Section 6**).
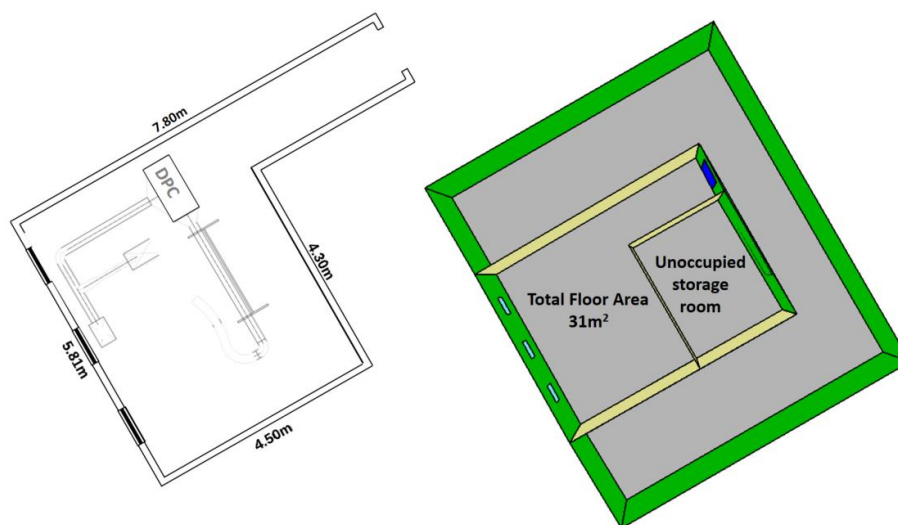
374

375 **Figure 5** Left: Floor plan of the laboratory room depicting DPC configuration, Right: Building

376 layout with adjacent rooms to the laboratory as modelled in DesignBuilder

377 The building hosting the Dew Point Cooler (DPC) in experiments was modelled in
378 EnergyPlus software package based on the data collected through a comprehensive survey
379 carried out on the building. **Figure 5** presents the floor plan of the laboratory building with
380 DPC test set-up, and a 2-D view of the building model.

381 As seen in **Figure 5** the adjacent spaces to the experiment room is also modelled in order to
382 capture possible impact they can have on the indoor environment of the laboratory and
383 consequently on system performance. The experiment room has total floor area of 31m^2 and
384 floor to ceiling height of 2.7m with an L-shaped layout, three windows with total glazing area
385 of 1.1m^2 and a wooden entrance door with area of 1.6m^2. **Table 6** summarises the
386 construction materials of the building, their compositions and their corresponding U-values
387 as modelled in EnergyPlus. Since the construction details of the building wasn't a part of
388 analysis in previous experimental or numerical modelling studies, the required details for
389 developing the whole building energy model was gathered separately by surveying the
390 building envelope and referring to building plans and construction handbook provided by
391 states office at the University of Hull, where the DPC is tested. Hence, the description of
392 construction materials and details of their layers were used in the modelling process and
393 resultant U-values are reported in **Table 6**.

394 The external walls are made of lightweight concrete blocks as outermost layers followed by a
395 thin air gap and plasterboard on the inside of the building, with an overall U-value of 1.6
396 W/m^{2}K. The laboratory where the experiments were carried out was located on second floor
397 of the building, hence the internal floor and ceiling was modelled as a solid concrete slab
398 with U-value of 0.7 W/m^{2}K. The room has three square windows, equally spaced on the
399 external wall with single glazing and aluminium frame which were closed during the
400 experiments and hence modelled with zero opening area and overall U-value of 4.8 W/m^{2}K.
401 The entrance door to the room was a wooden one with 65mm thickness and U-value of 3.0
402 W/m^{2}K. Finally, the internal partitions separating the experiment room from the rest of
403 building were formed of a single layer brickwork covered with plaster on each side giving the
404 walls a thickness of 220mm and U-value of 2.1 W/m^{2}K.

405 Measuring infiltration rates of the experiment room was not possible at the time of this study
406 as the tests were running in the experiment room. Instead, airtightness test results of a
407 similar laboratory in the same building which was carried out in 2017 and reported in building
408 data repository was used. The airtightness test was carried out with 50 Pa pressurised unit
409 and **Equation 9**, from BS EN 12831 [47] was used to convert the reported value to
410 infiltration rate at normal operating conditions:

$$\dot{V}_{inf,i} = 2 \times V_i \times n_{50} \times e_i \times \varepsilon_i \qquad \qquad \textbf{Equation 9}$$

411   Where $\dot{V}_{inf,i}$ is the infiltration rate of the space, V_i is the volume of space (m³), n_{50} is the air

412   exchange rate per hour (ACH), resulting from a pressure difference of 50 Pa between the

413   inside and outside of the building, e_i is the shielding factor which was taken as 0.03 for a

414   moderate shielding and heated spaces with more than one exposed opening, and ε_i is

415   height correction factor which takes into account the increase in wind speed with the height

416   of the space from ground level. $\varepsilon_i = 1$ when the centre of zone height to ground level is

417   below 10m which was the case in the experiment room. Inserting the infiltration value of 0.16

418   ACH (as result of airtightness test) into the **Equation 9**, an infiltration rate of 0.8 ACH was

419   calculated and added to the whole building energy model of the building.

420   **Table 6** Summary of construction materials as modelled in EnergyPlus, physical properties,
421   and corresponding overall U-values

Element	Description	Layers	Thickness (mm)	Density (kg/m³)	Specific heat capacity (J/kgK)	U-value (W/m²K)
External walls	Lightweight concrete block, air gap and plasterboard	Concrete block	200	600	1000	1.6
		Air gap	25	-	-	
		Steel	10	7800	450	
		Plasterboard	10	900	1000	
Internal floor/ceiling	Solid (concrete slab)	Cast concrete	150	2100	840	0.7
Windows	Single glazing with aluminium frame	Glazing	3	-	-	4.8
		Frame	35	2800	880	
Entrance door	Wooden	Painted oak	65	700	2390	3.0
Internal partitions	Solid Brick	Brick (inner)	220	1700	1000	2.1

422   The building was modelled as two thermals zones: the experiment room and the rest of the

423   building. The heat gains from the system equipment were excluded from the zone definition

424   as these details are included in the system model and the resultant impact on system

425   performance and indoor environment is considered. The occupancy and the metabolic gains

426   are also modelled to represent presence of a single person (to run the experiments) in the

427   room during system operations and no window or door opening is considered to eliminate

428   the impact of external air flow on system performance. Lighting gains of 10 W/m² are also

429   considered in the model.

430   The custom EnergyPlus weather files were created by scaling typical weather year data from

431   the International Weather for Energy Calculations (IWEC) [48] following the methodology

432   described in a previous article by the authors [49]. Monthly values of external air temperature

433   and relative humidity were compared with the experimental weather values to produce a

434   scaling factor. The scaling factor was then applied to the hourly values using EnergyPlus

435   auxiliary weather programme [46] to produce equivalent weather information suitable for

436   whole building energy modelling. For weather information from Beijing and Rome, the pre-

437   treated values given in **Table 3** were used to develop the equivalent hourly weather file,

438   whereas for Riyadh and Las Vegas the original values were used as no pre-treatment was

439   found necessary.

440   The DPC was modelled explicitly in EnergyPlus by detailed modification of the IDFs

441   including geometry and construction details. The dimension and size details of the system,

442   as presented in **Figure 6**, were added into IDFs as object-oriented entries which sat in the

443   previously allocated lines of the IDF as assigned by the system template.
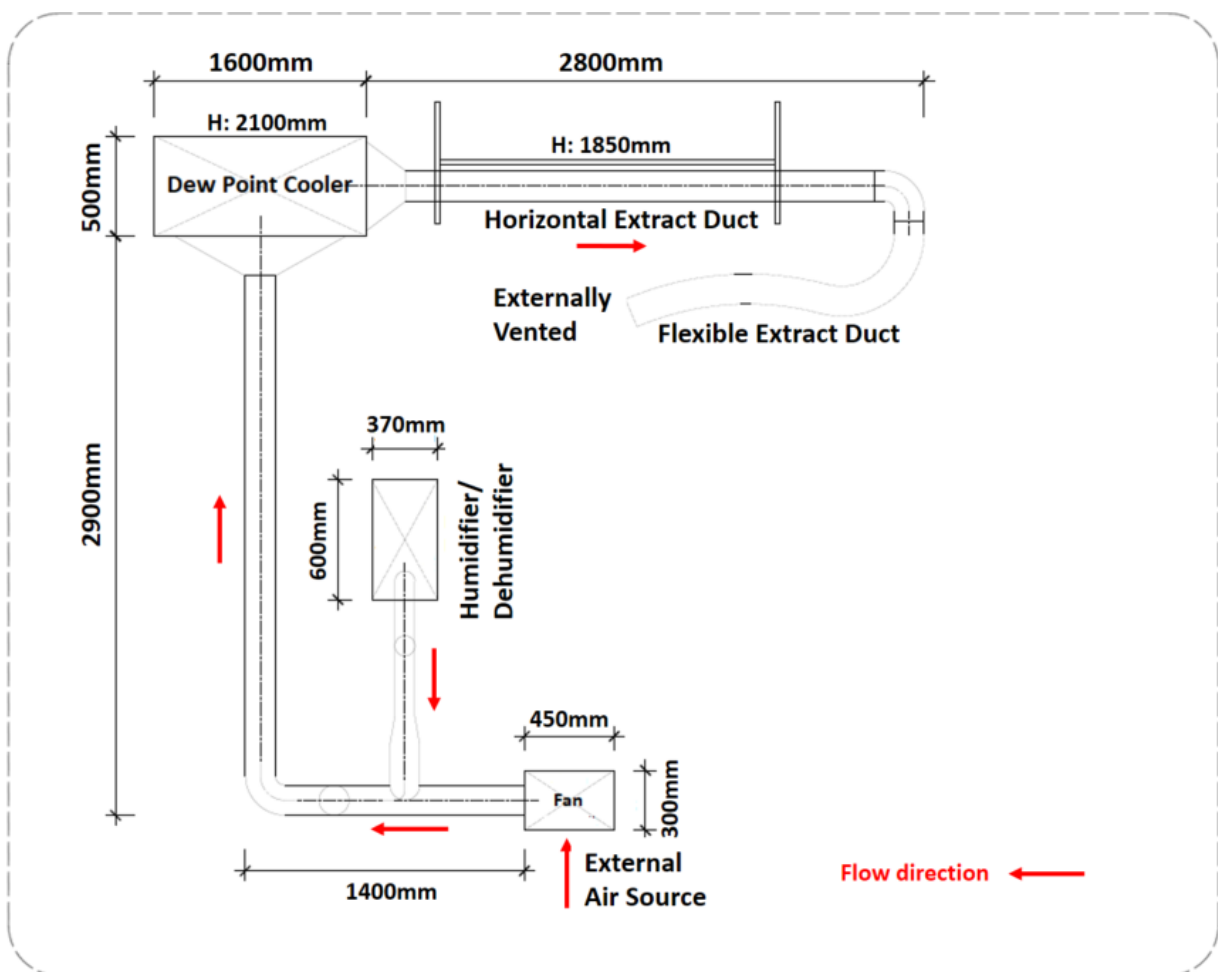
444

445   **Figure 6** Dew Point Cooler (DPC) and test set-up technical plan as constructed in laboratory

446   environment with component dimensions

447   The overall power requirements of the pumps and fans (90.5 W), pressure rise range and

448   efficiencies as identified in product catalogues, air flow rates passing through the wet and

449   dry channels of the DPC as measured in the experiments (602 and 364 $m^3.h^{-1}$), and height

450   of air inlets (2.1m) and outlets (1.85m) as depicted in **Figure 6** were all included the IDFs to

451   ensure system model is capable of simulating real-life operation of the DPC.

452   The details of the system as constructed in the laboratory environment was input explicitly

453   into IDFs except for the Thermal Mass Parameter (TMP). This was due to EnergyPlus not

454   having the capacity to model system physically, instead the operation and performance of

455   the system was modelled. Hence, the experiment room was modelled as a vacant space

456   with conditioned air inlet and exhaust air outlets. To account for the TMP of system

457   component, a further TMP of 50 kJ/m^2K was added to the existing TMP of the building as

458   calculated from **Equation 10** [50]:

$$TMP = \frac{\sum \kappa \times A}{TFA}$$
        Equation 10

459   Where κ is the heat capacity (kJ/m^2K) of each element, *A* is the element's area, and *TFA* is

460   the Total Floor Area of the experiment room, and the summation is over all walls together

461   with both sides of all internal walls and floors/ceilings.

462   **6. Results and Discussion**

463   *6.1. Comparison of the whole building energy model results with experiments:*

464   *empirical validation*

465   The completed IDFs which were developed to represent the actual system and hosting

466   building's characteristics under equivalent experimental conditions were fed to the

467   EnergyPlus calculation engine and simulations were run for the previously identified climates

468   (see **Table 3** for climate details). The model was calibrated and simulations were compared

469   to experimental results in order to validate the model. All the simulations were run in

470   EnergyPlus version 8.9.0.1, and simulation of system operation under each climate required

471   approximately 18 minutes of single CPU time for a full year simulation at 1-minute time

472   steps. The model was calibrated using the operational parameters contributing to cooling

473   capacity of the system, as provided in **Equation 1**. The specific heat capacity of the inlet air

474   (C_p), the inlet and outlet temperatures of the air in dry channel ($T_{dry,in}$ and $T_{dry,out}$), and the

475   working air to intake air ratio (φ) as modelled in EnergyPlus were checked against

476   experimental values to ensure system model characteristics matched those of the actual

477   system. Having calibrated the system model, simulation results were exported and analysed.
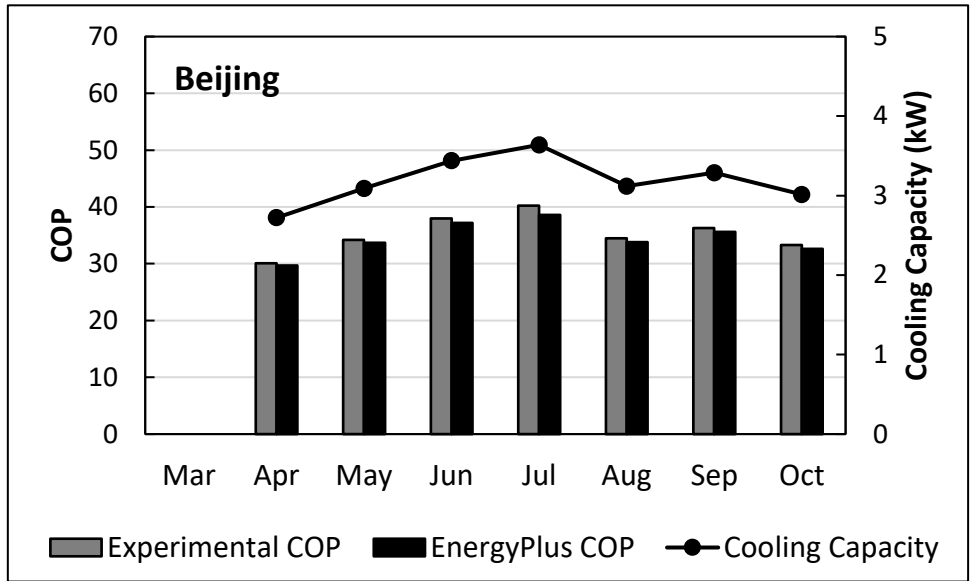
478   Figure 7 presents the comparison of experimental COP and cooling capacity results to

479   EnergyPlus predictions in: (a) Beijing, (b) Rome, (c) Las Vegas, and (d) Riyadh. As seen in

480   Figure 7, the cooling capacity of the actual system and simulations are identical to each

481   other in all the simulated climates. This shows that the calibration of model using the

482   mentioned operational parameters were reflected in the simulation results and the system

483   model is capable of representing actual operation of the DPC. However, other performance

484   parameters (as listed in **Table 4**) need to be checked to ensure that the whole building

485   energy model is also accurate and capable of representing transient interaction of the

486   system with surrounding building.

487   An initial look at the graphs in **Figure 7** reveals that both experimental and simulation values

488   of the COP in all four of the climates follow a similar trend to cooling capacity variations

489   throughout the year. The highest cooling capacity of the system and thus the highest power

490   consumption was observed under hot desert weather conditions of the Riyadh and

491   subtropical hot desert weather conditions of Las Vegas with cooling capacity reaching a

492   peak of 4.6 kW in July.

493   The DPC was required to run for 180 minutes under each weather condition to allow system

494   enough time to stabilize, and the rate of power consumption in Beijing, Rome, Las Vegas,

495   and Riyadh as recorded by experiments were 12.77 kW, 10.21 kW, 13.56 kW, and 15.33

496   kW, respectively. In this study, the rate of power consumption by DPC under different

497   weather conditions is considered instead of the amount of used electricity as the comparison

498   factor. This is mainly because of different running times of the DPC in various regions and

499   hosting facilities which are highly dependent on the weather conditions and the amount of

500   dissipated heat as well as various operating time of facilities. Hence, the rate of power

501   consumption was chosen as comparison factor in order to eliminate impact of inequivalent

502   operating parameters on system performance. Considering the 24-hour operation of DPC

503   during the operating months (as indicated in **Table 3**), the estimated annual consumption

504   values for Beijing, Rome, Las Vegas and Riyadh become 64.4 MWh, 44.1 MWh, 68.3 MWh,

505   and 88.3 MWh, respectively.

506   In case of COPs, the highest values were recorded both by experiments and simulations in

507   four consecutive months (June-September) of Riyadh, reaching experimental peak of 51.1

508   and simulation peak of 49 in July. The lowest COP values, on the other hand, were observed

509   both experimentally (17.7) and by simulation (17.9) in April of Las Vegas. The COP and

510   cooling capacity values in all the climates show an increasing trend towards warmer months

511   of the year and decreasing trends in relatively cooler months. These trends are well justified,
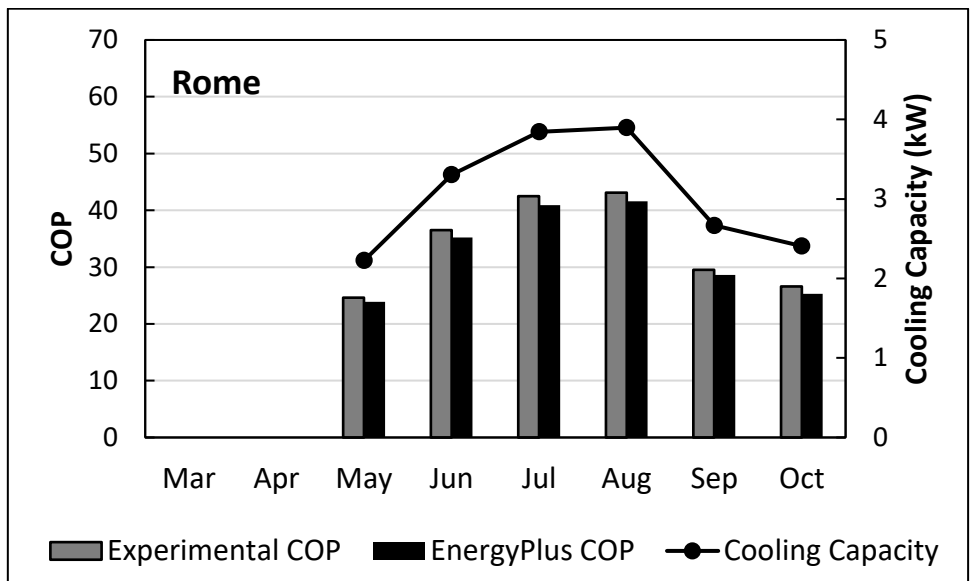
512   considering that both cooling capacity and COP are dependent on external weather

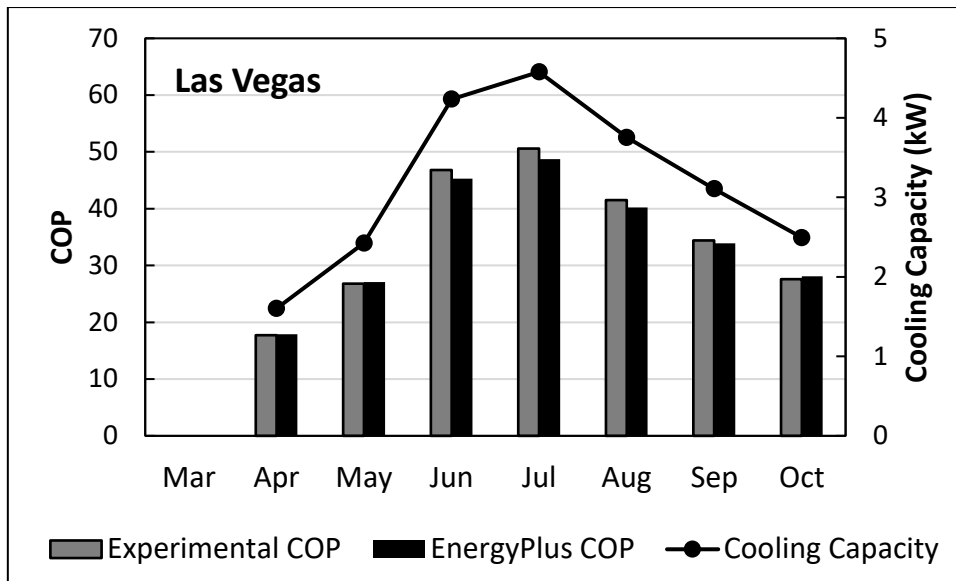513   conditions (**Equation 1** and **Equation 2**).
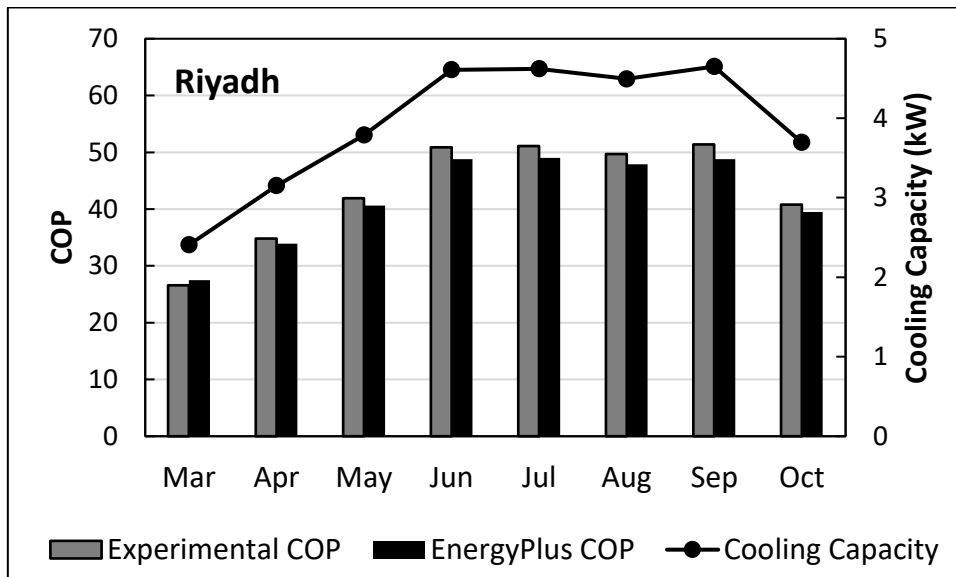
514

515   (a)

516

517   (b)

(c)

(d)
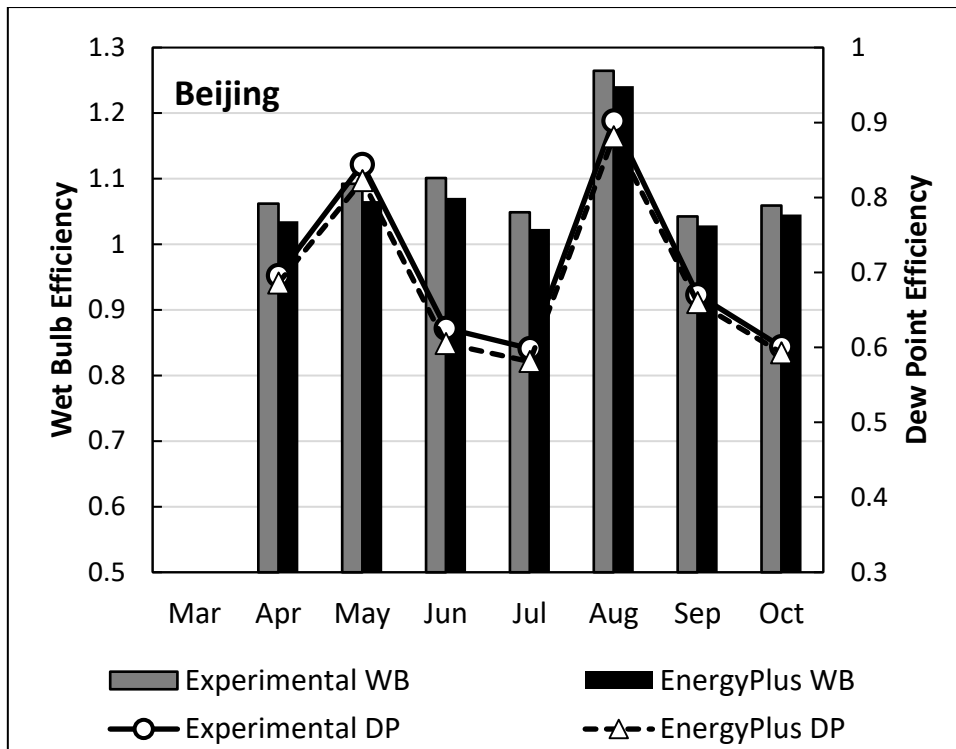
Figure 7 Comparison of experimental COP and cooling capacity results to EnergyPlus predictions in: (a) Beijing, (b) Rome, (c) Las Vegas, and (d) Riyadh

Upon careful calibration of the model, it can be seen in **Figure 7** that experimental COP results and simulation predictions are in good agreement with a maximum recorded error of 4.13% and mean error of 3.65% in Riyadh, as summarised in **Table 7**. The best fit between experiments and simulations is achieved in Beijing with mean error of 2.13% followed by Las Vegas and Rome with mean errors of 2.23% and 3.6%, respectively (**Table 7**). The simulations predict lower COP values compared to experiment results in majority of the months, except for April and May in Las Vegas and March in Riyadh where the whole

building energy model over-estimated the COP values. This can be related to the sensitivity of model to lower external temperatures and relatively low COP values in these months (<30). With higher COP values, the model tends to predict higher COP values compared to experiment results.

Figure 8 presents the other two performance parameters of the DPC, namely the wet bulb and dew point efficiencies, which are calculated based on inlet and outlet temperatures of the system (**Equation 3** and Equation 4). As can be seen in **Figure 8**, the experimental and simulation values for both wet bulb and dew point efficiencies, in all investigated climates, are in good agreement and are following similar trends throughout the year. A look at the error values in **Table 7** reveals that, similar to COP predictions, EnergyPlus has successfully predicted the efficiencies of the system, presenting a robust case for model validation. The largest monthly difference observed between EnergyPlus and experimental results of the wet bulb and dew point efficiency are 5% (July in Rome) and 4.3% (July in Las Vegas), respectively. Overall, the whole building energy model gave the best predictions of efficiency parameters for Beijing and Las Vegas with mean error values of below 2.5%. The efficiency predictions for Las Vegas and Riyadh, despite being in validation range, showed a larger gap between experimental and simulation results with mean errors of 3.5-3.7%, as seen in **Table 7**.

The closer investigation of the results in Figure 8, shows that both experimental and simulation results of the efficiency parameters have a steadier rate of variation in Riyadh compared to the other three climates, and hence the DPC performs at a more steady and reliable state. Such stability of operation can be related to two main factors: (i) that the mean monthly external air temperatures, which is fed to the system as working air, has less variations in Riyadh compared to the other investigated climates; and (ii) the Riyadh weather, as a hot desert climate, has the least amount of water content (i.e. humidity) compared to Beijing, Rome and Las Vegas (as seen in **Table 3**). Hence, the statement (supported by both experiments and validated whole building energy model) can be made that the dew point evaporative coolers tend to have more reliable and steady performance in hot desert climates. Such reliable and steady operation of the system, especially in high demand facilities like data centres plays a key role in effective energy management and provides flexibility in dealing with peaks of power consumption. Therefore, it can be concluded that, although higher efficiencies and COP values can be reached in some months of more moderate and humid climates, the sustained and steady operation of the investigated system is achieved in hot and dry climates.
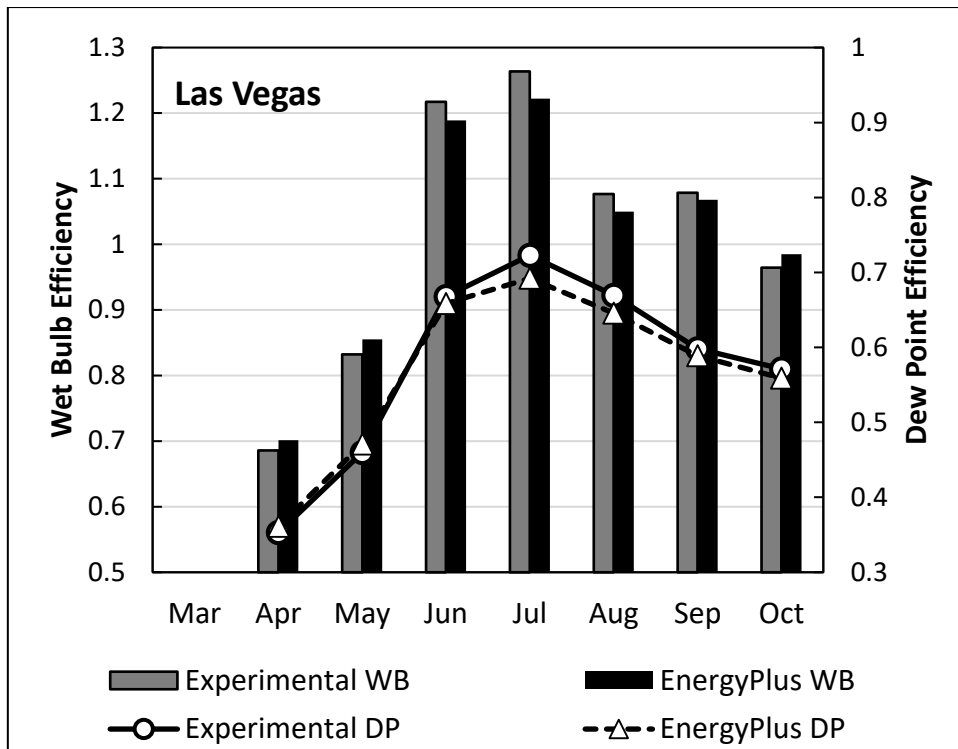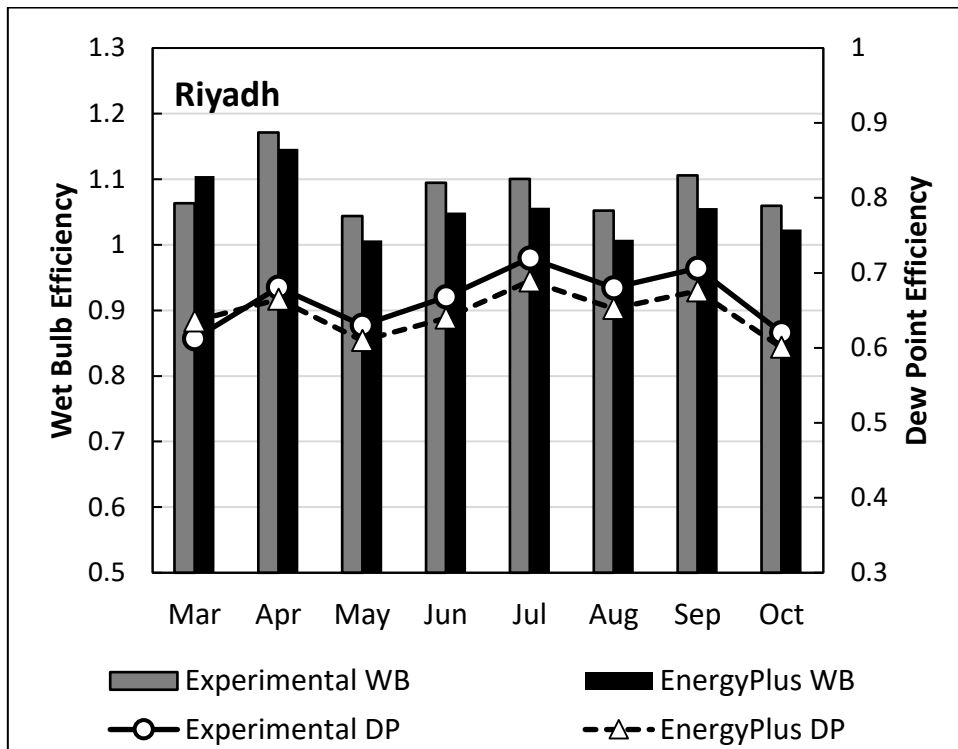
(a)

(b)

565

566

567

568

(c)

(d)
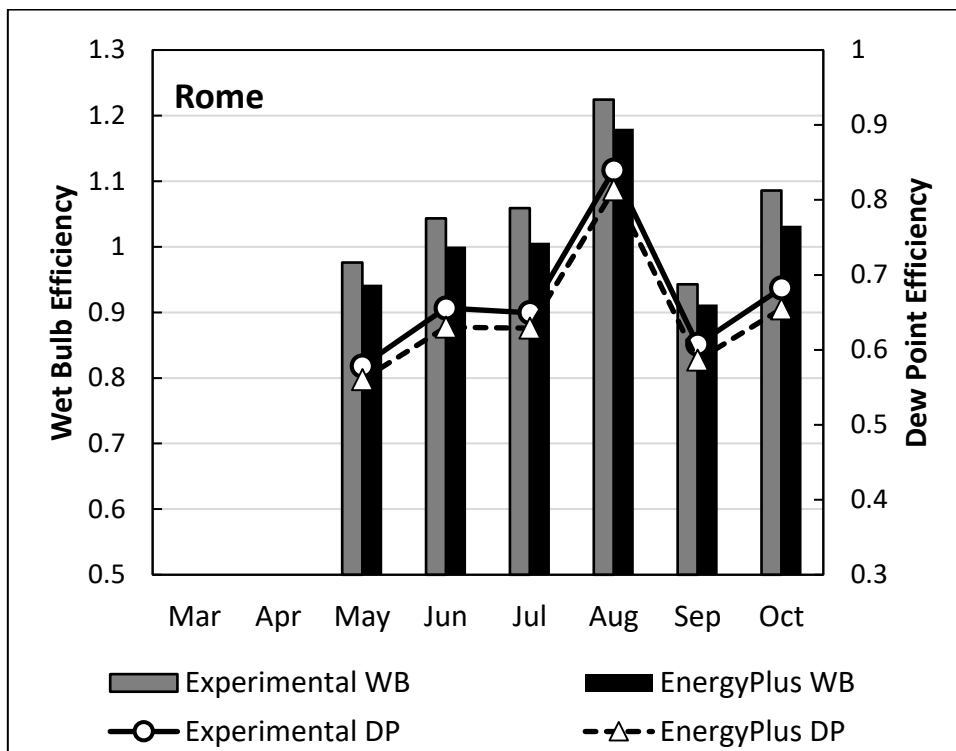
Figure 8 Comparison of experimental wet bulb and dew point efficiencies to EnergyPlus predictions in: (a) Beijing, (b) Rome, (c) Las Vegas, and (d) Riyadh

575 **Table 7** Monthly and average difference between experimental values of COP, wet bulb and
576 dew point efficiencies with EnergyPlus predictions

| City	Month	COP Error (%)	Mean COP Error (%)	Wet Bulb Efficiency Error (%)	Mean Wet Bulb Efficiency Error (%)	Dew Point Efficiency Error (%)	Mean Dew-Point Efficiency Error (%)
Beijing	March	-		-		-	
	April	1.3289		2.5424		1.4799	
	May	1.4620		2.4350		2.5570	
	June	2.1053		2.7611		3.2614	
	July	3.9801	2.1337	2.4123	2.0921	2.8911	2.2109
	August	2.0290		1.8582		2.3390	
	September	1.9284		1.3427		1.5813	
	October	2.1021		1.2933		1.3643	
Rome	March	-		-		-	
	April	-		-		-	
	May	2.8455		3.4532		3.1460	
	June	3.5616		4.1115		3.9042	
	July	3.7647	3.5984	4.9679	4.0664	3.1717	3.4793
	August	3.4803		3.6269		3.1201	
	September	3.0509		3.2665		3.4744	
	October	4.8872		4.9724		4.0592	
Las Vegas	March	-		-		-	
	April	-1.1299		-2.3042		-2.3519	
	May	-1.1194		-2.7761		-2.4571	
	June	3.2051		2.3334		1.3627	
	July	3.7549	2.2296	3.2996	2.3453	4.2474	2.5300
	August	3.1325		2.5258		3.5842	
	September	1.4535		1.0105		1.5714	
	October	-1.8116		-2.1676		2.1351	
Riyadh	March	-3.3835		-3.9413		-3.8556	
	April	2.5862		2.1431		2.2921	
	May	3.1026		3.5642		3.2688	
	June	4.1257		4.1301		4.2079	
	July	4.1096	3.6468	3.9891	3.7432	4.2379	3.6714
	August	3.6217		4.2391		4.0435	
	September	5.0584		4.5035		4.3053	
	October	3.1863		3.4353		3.1603	

577

578

579

6.2. Comparison of the whole building energy model results with numerical model:
superiority analysis

In this section, the whole building energy model is compared to a previously developed numerical model of the same Dew Point Cooler (DPC) [38]. The 8th degree polynomial numerical model (described in **Section 4**) investigated the same cooling system and used the equivalent input parameters as employed by the whole building energy model. Despite the modelling work presented in this study, the numerical model lacks empirical validation and only involves an inter-model comparison to verify the results. Hence, this study offers an unprecedented opportunity to compare performance of a empirically validated whole building energy model, which takes into account the dynamic interaction of the system components with each other and also the interactions of the system with its surrounding building, to a commonly used numerical model; and provide evidence based and critical review of various modelling approaches.

The numerical model was developed based on 7857 possible operating conditions, majority of which doesn't happen in real-life operation of the system and only were considered to fully train the model [38]. The performance of the numerical model, after completing the training process was tested in the Las Vegas weather conditions, and hence here only a comparison of experiment results and models' predictions for the city of Las Vegas (Figure 9 and **Figure 10**) is presented. As can be seen in **Figure 9**, the unrestrained operating conditions employed by the numerical model can lead to COP estimates of up to two times higher than experimental values and EnergyPlus predictions. The numerical model has predicted different cooling capacities compared to the EnergyPlus and the experiments. The main reason for this lies in **Equation 1**, which shows that the cooling load is calculated based on operating parameters (various operating temperatures in this case) which has not be restricted reasonably by the numerical model. Hence, while the matching fan and pump powers are used in both models and the experiments, due to un-restricted operation parameters used by the numerical model, different cooling capacities and consequently different COPs have been predicted by the numerical model. The unrealistic COPs of 100 in June and July as estimated by the numerical model, highlights the critical need for models to take into account the restricting impact of parameters outside system operational conditions, i.e. interaction of the system with hosting building and surrounding environment. The numerical model over-estimates the COP of the system in all of the months that system was operated. The cooling capacity, however, shows a totally biased trend as it is over-estimated by the numerical model in March and April, under-estimated in May, June and July, and closely matches the experimental and EnergyPlus results in August and September (**Figure 9**).

616 Considering that the COP values are directly co-related to cooling capacity (**Equation 1** and
617 **Equation 2**), it is expected that the estimates of the two performance parameters by the
618 numerical model follow a similar trend when compared to experimental and real-life
619 performance parameters of the system. However, the larger overall difference observed in
620 COP estimates than the cooling capacity estimates of the numerical model when compared
621 to experimental values suggests that the numerical model is more sensitive to cooling
622 capacity variances when it comes to COP calculations.
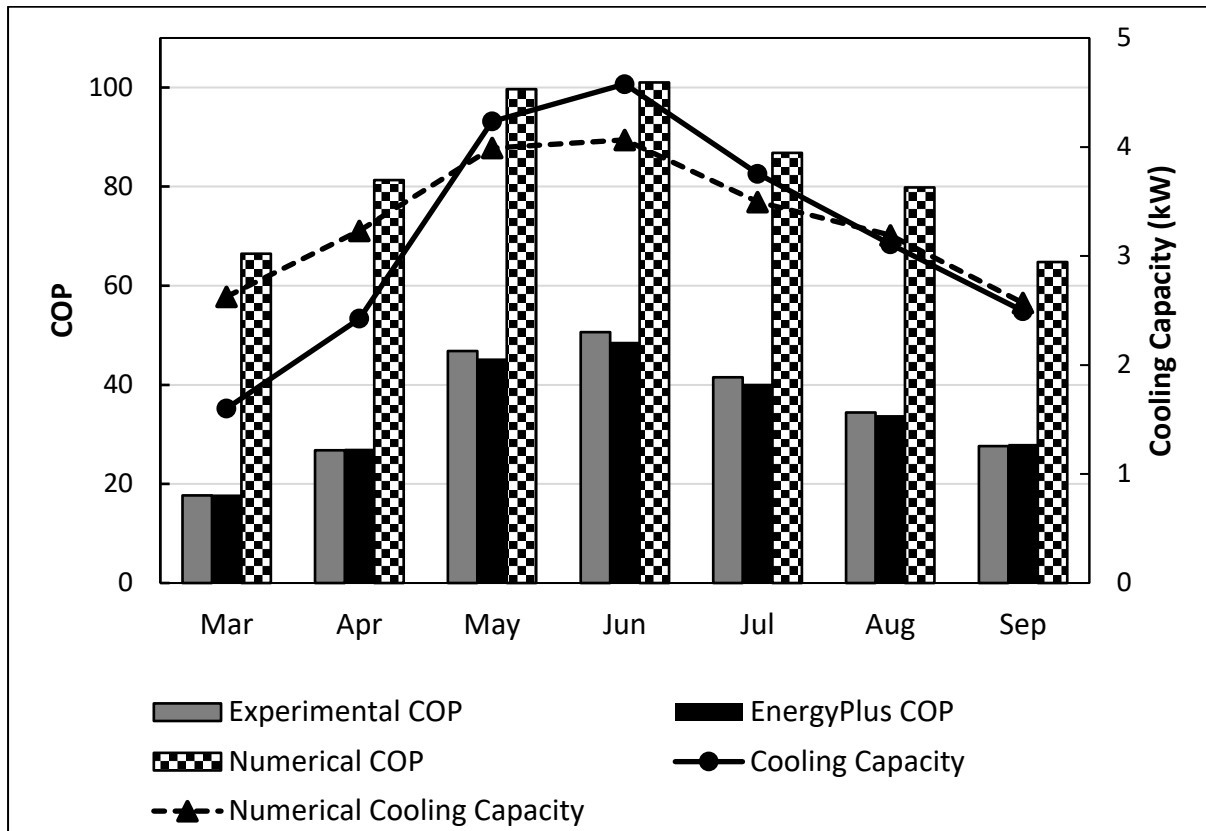
624 **Figure 9** Comparison of cooling capacity and COP from experiments and EnergyPlus to
625 numerical model estimates in Las Vegas

626 Investigating the wet bulb and dew point efficiency estimates of the numerical model (**Figure**
627 **10**) shows that, similar to COP values, the numerical model over-estimates both efficiency
628 values. The smallest differences between the experimental and numerical model results are
629 recorded in May and June, and the largest difference in March and April. **Figure 10** clearly
630 shows that while the validated EnergyPlus model predicts very close efficiencies to the
631 experiments, the numerical model fails to produce realistic efficiency predictions in most
632 months. The close agreement of numerical model estimates in May and June shows that the
633 operating parameters used in these months match with the realistic values, whereas in

634 March and April the trained operating parameters are far from reality, resulting in poor

635 prediction of the wet bulb and dew point efficiencies.

636 The randomness of the variances in numerical model errors compared to experiments and

637 EnergyPlus results, as observed in Figure 9 and **Figure 10**, increases the confidence in

638 concluding that the characteristics difference of the models in simulating operation of the

639 DPC causes the recorded differences with real life operation of the system. Especially that

640 the two models (EnergyPlus and numerical) used equivalent and matching input parameters,

641 proves that the input parameters and unidentified uncertainties didn't have role in poor

642 performance of the numerical model.

643
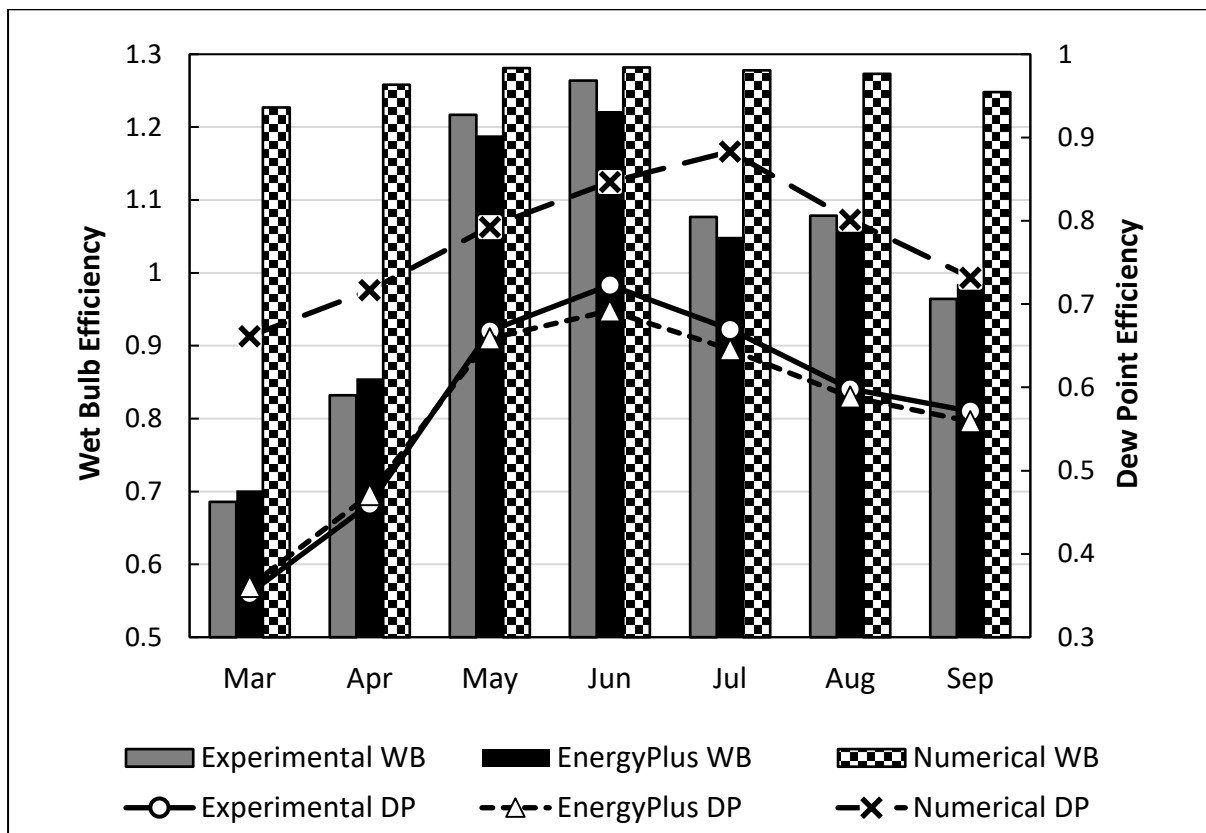
Figure 10 Comparison of wet bulb and dew point efficiencies from experiments and
645 EnergyPlus to numerical model estimates in Las Vegas

646 Having compared the whole building energy model and numerical model predictions with

647 each other and with real-life experimental results revealed that despite numerical models'

648 capacities in swift assessment of evaporative cooling system, these models fail to take into

649 account the various restraining parameters which would lower the performance parameters

650 of the investigates system. Hence, the numerical models tend to over-estimate the key

651 performance parameters like COP, wet bulb and dew point efficiencies resulting in

652 unrealistic and biased assessment of the system performance. The whole building energy

653 model developed in this study proved to better predict the performance of dew point
654 evaporative cooler by incorporating the building-side parameters into the model and showing
655 very close agreement with experimental performance parameters of the system.

656 Hence, the authors conclude with high certainty that validated whole building energy models
657 can outperform numerical models in assessing performance of dew point evaporative
658 coolers. These models also provide a great opportunity to investigate the system
659 performance in a wide range of hosting buildings, from commercial buildings to schools,
660 hospitals and office buildings, providing valuable insight into the necessary modification that
661 might be necessary before operating the system in various buildings.

662 **7. Conclusion**

663 Faced with increasing interest in Indirect Evaporative Coolers (IECs) as a popular low
664 energy cooling solution for high demand facilities, this study performed a modelling and
665 experimental investigation of a state-of-the-art indirect dew point evaporative cooler. The
666 investigated system was a high-performance counter flow Dew Point Cooler (DPC)
667 employing a guideless and corrugated Heat and Mass Exchanger (HMX) as described in
668 **Section 2**. The experiments were run under four different weather conditions: Beijing as
669 humid continental climate, Rome as Mediterranean climate, Las Vegas as subtropical hot
670 desert climate, and Riyadh as hot desert climate investigating four key performance
671 parameters of the DPC: (i) cooling capacity, (ii) Coefficient of Performance (COP), (iii) wet
672 bulb efficiency, and (iv) dew point efficiency (**Section 3**). The numerical model tested against
673 the experiments was an 8th degree Multiple Polynomial Regression (MPR) model employing
674 6561 operational parameters as the training set and 1296 operational parameters as the
675 validation set. The key operational parameters used in the numerical model were intake air
676 temperature, relative humidity, and flow rate as well as Working air to intake air ratio
677 (**Section 4**). The whole building energy model of the system and the hosting building was
678 developed in the EnergyPlus software package which is an internationally known and tested
679 tool for building energy simulation. The model was calibrated and validated empirically using
680 experimental results (**Section 5**). The whole building energy model results were compared
681 to experiments as part of model calibration and validation. The validated model was then
682 compared to the numerical model to investigate superiority of the two approaches in
683 predicting performance of advance dew point evaporative coolers (**Section 6**). The key
684 findings and conclusions of the study can be summarised as:

685 • The highest power consumption was observed under hot desert weather conditions of
686   the Riyadh (15.33 kW) and subtropical hot desert weather conditions of Las Vegas
687   (13.56 kW) with cooling capacity reaching a peak of 4.6 kW in July.

- The highest COP values were recorded both by experiments and whole building energy simulations in four consecutive months (June-September) of Riyadh, reaching experimental peak of 51.1 and simulation peak of 49 in July.
- The lowest COP values were observed both experimentally (17.7) and by simulation (17.9) in April of Las Vegas.
- Experimental COP results and whole building energy simulation predictions were in good agreement with a maximum recorded error of 4.13% and mean error of 3.65% in Riyadh.
- The best COP fit between experiments and whole building energy simulations was achieved in Beijing with mean error of 2.13% followed by Las Vegas and Rome with mean errors of 2.23% and 3.6%, respectively.
- The largest difference observed between EnergyPlus and experimental results of the wet bulb and dew point efficiency are 5% (July in Rome) and 4.3% (July in Las Vegas), respectively.
- The whole building energy model gave the best predictions of efficiency parameters for Beijing and Las Vegas with mean error values of below 2.5%. The efficiency predictions for Las Vegas and Riyadh, despite being in validation range, showed a larger gap between experimental and simulation results with mean errors of 3.5-3.7%.
- The unrestrained operating conditions employed by the numerical model lead to COP estimates of up to two time higher than experimental values and EnergyPlus predictions. The numerical model over-estimates both efficiency values.
- The whole building energy model proved to better predict the performance of dew point evaporative cooler by incorporating the building-side parameters into the model.

This study proved that comprehensive validation of the numerical model (and generally any model) is a crucial part of any modelling exercise in achieving the most reliable predictions. Hence, the future work by authors will focus on developing hybrid numerical models which take into account the building side parameters and use the data from whole building energy models where necessary to develop robust numerical models capable of representing reality with high precision.

Acknowledgments

References

722 [1]   IEA, "World Energy Outlook," 2019. [Online]. Available: https://www.iea.org/weo2019/.
723   [Accessed: 02-Dec-2019].

724 [2]   L. Perez-Lombard, J. Ortiz, and C. Pout, "A review on buildings energy consumption
725   information ´," *Energy Build.*, vol. 40, pp. 394–398, 2008.

726 [3]   K. J. Chua, S. K. Chou, W. M. Yang, and J. Yan, "Achieving better energy-efficient air
727   conditioning – A review of technologies and strategies," *Appl. Energy*, vol. 104, pp.
728   87–104, 2013.

729 [4]   P. Xu, X. Ma, X. Zhao, and K. Fancey, "Experimental investigation of a super
730   performance dew point air cooler," *Appl. Energy*, vol. 203, pp. 761–777, 2017.

731 [5]   M. I. Isaac and D. P. Van Vuuren, "Modeling global residential sector energy demand
732   for heating and air conditioning in the context of climate change," vol. 37, pp. 507–
733   521, 2009.

734 [6]   M. Scott and Y. Huang, "Annex A: Technical note: methods for estimating energy
735   consumption in buildings in effects of climate change on energy production and use in
736   the United States. A Report by the U.S. climate change science program and the
737   subcommittee on global change resea," Washington (DC), 2007.

738 [7]   Y. Huang, "The impact of climate change on the energy use of the U.S. residential
739   and commercial building sectors," Lawrence Berkeley National Laboratory, Berkeley
740   (CA), 2006.

741 [8]   T. Frank, "Climate change impacts on building heating and cooling energy demand in
742   Switzerland," vol. 37, pp. 1175–1185, 2005.

743 [9]   X. Wang, M. Zheng, W. Zhang, S. Zhang, and T. Yang, "Experimental study of a
744   solar-assisted ground-coupled heat pump system with solar seasonal thermal storage
745   in severe cold areas," *Energy Build.*, vol. 42, no. 11, pp. 2104–2110, 2010.

746 [10] L. Z. Zhang, "Energy performance of independent air dehumidification systems with
747   energy recovery measures," vol. 31, pp. 1228–1242, 2006.

748 [11] K. Daou, R. Z. Wang, and Z. Z. Xia, "Desiccant cooling air conditioning : a review,"
749   vol. 10, pp. 55–77, 2006.

750 [12] V. Maisotsenko, "M-CYCLE (Indirect Evaporative Cooling)," 2007. [Online]. Available:
751   http://www.rexresearch.com/maisotsenko/maisotsenko.htm. [Accessed: 03-Dec-
752   2019].

753 [13] E. V. Gómez, A. T. González, F. Javier, and R. Martínez, "Experimental

754 characterisation of an indirect evaporative cooling prototype in two operating modes,"
755 vol. 97, pp. 340–346, 2012.

756 [14] H. Campaniço, P. Hollmuller, and P. M. M. Soares, "Assessing energy savings in
757 cooling demand of buildings using passive cooling systems based on ventilation," vol.
758 134, pp. 426–438, 2014.

759 [15] G. P. Maheshwari and R. K. Suri, "Energy-saving potential of an indirect evaporative
760 cooler," vol. 69, pp. 69–76, 2001.

761 [16] L. Elberling, "Laboratory evaluation of the coolerado cooler-indirect evaporative
762 cooling unit," Pacific Gas and Electric Company, 2006.

763 [17] N. J. Stoitchkov and G. I. Dimitrov, "Effectiveness of crossflow plate heat exchanger
764 for indirect evaporative cooling ´ des e ´ changeurs thermiques a ` plaques , a `
765 courants Efficacite ´ vaporatif croises pour refroidissement indirect e," vol. 21, no. 6,
766 pp. 463–471, 1998.

767 [18] X. Zhao, J. M. Li, and S. B. Riffat, "Numerical study of a novel counter-flow heat and
768 mass exchanger for dew point evaporative cooling," vol. 28, pp. 1942–1951, 2008.

769 [19] C. Zhan, Z. Duan, X. Zhao, S. Smith, H. Jin, and S. Riffat, "Comparative study of the
770 performance of the M-cycle counter- fl ow and cross- fl ow heat exchangers for
771 indirect evaporative cooling e Paving the path toward sustainable cooling of
772 buildings," *Energy*, vol. 36, no. 12, pp. 6790–6805, 2011.

773 [20] B. Riangvilaikul and S. Kumar, "An experimental study of a novel dew point
774 evaporative cooling system," *Energy Build.*, vol. 42, no. 5, pp. 637–644, 2010.

775 [21] F. Bruno, "On-site experimental testing of a novel dew point evaporative cooler,"
776 *Energy Build.*, vol. 43, no. 12, pp. 3475–3483, 2011.

777 [22] Y. Golizadeh, A. Badiei, X. Zhao, K. Aslansefat, X. Xiao, S. Shittu, X. Ma, "A
778 constraint multi-objective evolutionary optimization of a state-of-the-art dew point
779 cooler using digital twins" *Energy Convers. Manag.*, vol. 211, 2020.
780 https://doi.org/10.1016/j.enconman.2020.112772

781 [23] S. Moshari and G. Heidarinejad, "Numerical study of regenerative evaporative coolers
782 for sub-wet bulb cooling with cross- and counter- fl ow con fi guration," *Appl. Therm.*
783 *Eng.*, vol. 89, pp. 669–683, 2015.

784 [24] Y. Chen, H. Yang, and Y. Luo, "Parameter sensitivity analysis and configuration
785 optimization of indirect evaporative cooler (IEC) considering condensation," *Appl.*

786   *Energy*, vol. 194, pp. 440–453, 2017.

787   [25]   A. E. Kabeel and M. Abdelgaied, "Numerical and experimental investigation of a novel
788   configuration of indirect evaporative cooler with internal baffles," *Energy Convers.*
789   *Manag.*, vol. 126, pp. 526–536, 2016.

790   [26]   B. Riangvilaikul and S. Kumar, "Numerical study of a novel dew point evaporative
791   cooling system," *Energy Build.*, vol. 42, no. 11, pp. 2241–2250, 2010.

792   [27]   M. Jradi and S. Riffat, "Experimental and numerical investigation of a dew-point
793   cooling system for thermal comfort in buildings," *Appl. Energy*, vol. 132, pp. 524–535,
794   2014.

795   [28]   P. Xu *et al.*, "Numerical investigation of the energy performance of a guideless
796   irregular heat and mass exchanger with corrugated heat transfer surface for dew point
797   cooling," *Energy*, vol. 109, pp. 803–817, 2016.

798   [29]   P. Xu, X. Ma, X. Zhao, and K. S. Fancey, "Experimental investigation on performance
799   of fabrics for indirect evaporative cooling applications," *Build. Environ.*, vol. 110, pp.
800   104–114, 2016.

801   [30]   A. Hasan, "Going below the wet-bulb temperature by indirect evaporative cooling :
802   Analysis using a modified e -NTU method," *Appl. Energy*, vol. 89, no. 1, pp. 237–245,
803   2012.

804   [31]   J. Lin, K. Thu, T. D. Bui, R. Z. Wang, K. C. Ng, and K. J. Chua, "Study on dew point
805   evaporative cooling system with counter-flow configuration," vol. 109, pp. 153–165,
806   2016.

807   [32]   X. Cui, K. J. Chua, and W. M. Yang, "Numerical simulation of a novel energy-efficient
808   dew-point evaporative air cooler," *Appl. Energy*, vol. 136, pp. 979–988, 2014.

809   [33]   J. Lin *et al.*, "Unsteady-state analysis of a counter- fl ow dew point evaporative cooling
810   system," vol. 113, pp. 172–185, 2016.

811   [34]   D. Pandelidis and S. Anisimov, "Numerical analysis of the heat and mass transfer
812   processes in selected M-Cycle heat exchangers for the dew point evaporative
813   cooling," *Energy Convers. Manag.*, vol. 90, pp. 62–83, 2015.

814   [35]   D. Pandelidis and S. Anisimov, "Numerical study and optimization of the cross-flow
815   Maisotsenko cycle indirect evaporative air cooler," *Int. J. Heat Mass Transf.*, vol. 103,
816   pp. 1029–1041, 2016.

817   [36]   A. Sohani, H. Sayyaadi, and S. Hoseinpoori, "Modeling and multi-objective

818   optimization of an M-cycle cross-flow indirect evaporative cooler using the GMDH
819   type neural network Modélisation et optimisation à objectifs multiples d ' un
820   refroidisseur évaporatif indirect à écoulements croisés à cycle M en utilisant le réseau
821   neuronal de type GMDH," *Int. J. Refrig.*, vol. 69, pp. 186–204, 2016.

822 [37] X. Cui, K. J. Chua, W. M. Yang, K. C. Ng, K. Thu, and V. T. Nguyen, "Studying the
823   performance of an improved dew-point evaporative design for cooling application,"
824   vol. 63, pp. 624–633, 2014.

825 [38] Y. Golizadeh, X. Ma, X. Zhao, and S. Shittu, "A statistical model for dew point air
826   cooler based on the multiple polynomial regression approach," *Energy*, vol. 181, pp.
827   868–881, 2019.

828 [39] Y. Golizadeh, X. Zhao, S. Shittu, A. Badiei, M. E. G. V Cattaneo, and X. Ma,
829   "Statistical investigation of a dehumidification system performance using Gaussian
830   process regression," *Energy Build.*, vol. 202, p. 109406, 2019.

831 [40] ASHRAE, "American Society of Heating Refrigerating and Air-Conditioning Engineers:
832   Handbook of Fundamentals, SI edition," Atlanta, GA, USA, 2009.

833 [41] ASHRAE, "American Society of Heating Refrigerating and Air-Conditioning Engineers:
834   TC9.9 Data Center Power Equipment Thermal Guidelines and Best Practices,"
835   Atlanta, GA, USA, 2016.

836 [42] A. Pakari and S. Ghani, "Regression models for performance prediction of counter fl
837   ow dew point evaporative cooling systems," *Energy Convers. Manag.*, vol. 185, no.
838   November 2018, pp. 562–573, 2019.

839 [43] K. P. Moustris, P. T. Nastos, I. K. Larissi, and A. G. Paliatsos, "Application of Multiple
840   Linear Regression Models and Artificial Neural Networks on the Surface Ozone
841   Forecast in the Greater Athens Area , Greece," vol. 2012, 2012.

842 [44] NREL, "EnergyPlus Version 9.0.1," 2018. [Online]. Available:
843   https://github.com/NREL/EnergyPlus/releases/tag/v9.0.1. [Accessed: 07-Jan-2020].

844 [45] DesignBuilder, "DesignBuilder user manual Version 6. UK: DesignBuilder software
845   limited." [Online]. Available: https://designbuilder.co.uk/helpv6.0/. [Accessed: 07-Jan-
846   2020].

847 [46] EnergyPlus, "Auxiliary EnergyPlus Programs." [Online]. Available:
848   https://energyplus.net/sites/default/files/pdfs_v8.3.0/AuxiliaryPrograms.pdf.
849   [Accessed: 07-Jan-2020].

850 [47] BSI, "BS EN 12831: Heating systems in buildings — Method for calculation of the
851   design heat load. The British Standards Institution.," 2013.

852 [48] ASHRAE, "International weather for energy calculations. American Society of Heating,
853   Refrigerating and Air-Conditioning Engineers, Atlanta, GA, ASHRAE," 2001. [Online].
854   Available: https://www.ashrae.org/technical-resources/bookstore/ashrae-international-
855   weather-files-for-energy-calculations-2-0-iwec2. [Accessed: 09-Jan-2020].

856 [49] A. Badiei, D. Allinson, and K. J. Lomas, "Automated dynamic thermal simulation of
857   houses and housing stocks using readily available reduced data," Energy & Buildings
858   vol. 203, 2019. https://doi.org/10.1016/j.enbuild.2019.109431

859 [50] BRE, "The Government's Standard Assessment Procedure for Energy Rating of
860   Dwellings (SAP 2012). Garston, Watford, WD25 9XX, UK.," 2012. [Online]. Available:
861   https://www.bre.co.uk/filelibrary/SAP/2012/SAP-2012_9-92.pdf. [Accessed: 10-Jan-
862   2020].